Nanoparticles of lead sulfide in porous glasses prepared by the sol-gel method

RENATA REISFELD[1,*], TSIALA SARAIDAROV[1], HARRY MINTI[1], KRYSTYNA WODNICKA[2]

[1]Department of Inorganic and Analytical Chemistry, Hebrew University of Jerusalem, 91940 Jerusalem, Israel, e-mail: renata@vms.huji.ac.il.

[2]University of Mining and Metallurgy, al. Adama Mickiewicza 30, 30–059, Kraków, Poland.

PbS semiconductor nanoparticles were grown inside the matrices of zirconium oxide (ZrO_2) and zirconium-silica-polyurethane (ZSUR) prepared by the sol-gel method. Zirconium ormosil included polyurethane used to control the growth and aggregation of PbS nanoparticles. The new matrix allows the incorporation of up to 40% PbS forming a characteristic structure of dendrite by reacting lead acetate with ammonium thiocyanate in the sol-gel matrix. The sol precursors of the matrix for ZSUR contain ZrO_2 matrix solution, epoxy-silica-ormosil (ESOR) and diurethane siloxane (DURS) synthesized separately. The size of nanoparticles as determined by transmission electron microscopy (TEM) ranges between 2–4 nm for 20% PbS in zirconium oxide and 8–10 nm for 20% PbS in ZSUR matrices. The porosity of the glasses is determined using the nitrogen adsorption technique. The pore size for ZSUR doped with 2% of PbS as determined by BET is 1.54 nm. Quantum size effect was observed from the shifts of absorption and photoluminescence (PL).

Keywords: porous glassas, lead sulfide, zirconium-silica-polyurethane, optical properties.
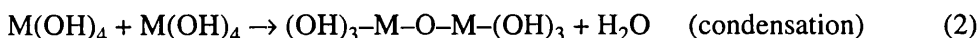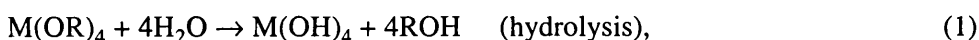
1. Introduction

The sol-gel technique offers a low temperature method for synthesizing amorphous materials which are either totally inorganic in nature or composed of inorganics and organics. The process is based on hydrolysis and polycondensation reactions of organometallic compounds in alcoholic solutions. The most widely investigated system involves silica-based glasses which are prepared by polymerization of silicon alkoxide $Si(OR)_4$ [1]–[5].

The process is based on inorganic polymerization reactions, starts from molecular precursors, and a macromolecular oxide network is obtained via hydroxylation condensation reactions which can be controlled by the chemical design of molecular precursors. The viscosity properties of sols can be adjusted allowing easy deposition

---

of transparent coatings onto glass, ceramic, or polymeric substrates. Sol-gel chemistry is performed in solution at lower temperatures than conventional chemical methods. Homogeneous doping by mixing components at a molecular level, synthesis of metastable or amorphous phases allowing larger concentrations of dopings, and synthesis of mixed organic-inorganic materials can then be performed.

In the case of organosilicate glasses (organically modified silicates or ormosils), the silicate network may be modified by organic substituents such as alkyl groups (*e.g.*, methyl) or other functional groups (*e.g.*, 3-glycidoxypropyl) which may form organic copolymers that penetrate the silicate structure. In principle, Si may be substituted by Al, B, Ti, or Zr to yield ceramics of variable mechanical properties [6]–[10]. A schematic representation of formation of oxide glass by the sol-gel method is:

$$M(OR)_4 + 4H_2O \rightarrow M(OH)_4 + 4ROH \quad \text{(hydrolysis)}, \tag{1}$$

$$M(OH)_4 + M(OH)_4 \rightarrow (OH)_3\text{–}M\text{–}O\text{–}M\text{–}(OH)_3 + H_2O \quad \text{(condensation)} \tag{2}$$

where M can be Si, Ti and Zr, and R is an alkyl group.

Semiconductor nanocrystals (NCs) incorporated in transparent media have received recently a large attention due to their promising applications in non-linear optics and optical switches. The incorporation of small semiconductor particles into thin films with wave guiding properties has potential applications in optoelectronics and optical integrated devices. Various semiconductor NCs have been prepared in the last two decades, either as dispersed colloidal particles in a liquid or solid matrix or in solid thin films. The incorporation of CdS and CdSe NCs into silica and zirconia (ZrO_2) films prepared by the sol-gel method has been reported previously [10]–[19]. The mostly studied semiconductor particles were cadmium sulfide [20]–[23]. The nonlinear properties of CdS incorporated in thin films prepared by the sol-gel method and in composite organic-inorganic polymers was described by us recently [22]. The preparation of the glasses doped by CdS was done in accordance with the general procedures of the preparation of glass films described in references. The thickness of the films is a function of the speed of the withdrawal of a substrate glass from the precursor solution, of pH, of the alkoxide concentration in the solution and of the sample orientation in respect to the direction of the withdrawal. The control of these conditions is necessary to guarantee reproducibility of the coatings. The sulfide resulting complex of Cd in the glass forms CdS particles of 20–30 Å size. The thickness of the films is determined by an interference method. CdS NCs exhibit a large optical non-linearity. However, their absorption edges appear at energies which are far from the telecommunication requirements.

More recent reports discuss also the incorporation of PbS NCs into glasses and polymers [24]–[29]. Lead sulfide is more suitable for telecommunication, because its bulk ground-state absorption edge located at 3100 nm (0.4 eV) can be shifted from near IR to the visible range, due to a quantum confinement effect of nanoparticles allowing large tunability. PbS NCs have been prepared and studied in a number of different sol-gel matrices [30]–[37]. The most widely investigated matrix materials

are SiO_2, ZrO_2, SiO_2/TiO_2, TiO_2/ormosil and ZrO_2/ormosil. PbS NCs of sizes 2–8 nm in ZrO_2 [31], [33], [35], 2–3.5 nm SiO_2/TiO_2 [34] and 4.8–10 nm in ZrO_2/ormosil matrix [30], [37] have been reported recently. Our present research has been focused on the synthesis and preparation of the PbS NCs and ZSUR films obtained by sol-gel processing. The purpose of the present work was to synthesize a new matrix material which can incorporate a wide range of PbS NCs concentrations. The matrix described below possesses the high mechanical and thermal stability and high refractive index due to the component zirconium oxide. The novel ormocer hybrid material was obtained by using three complexed precursors:

– DURS where poly(ethylene)glycol chain is covalently linked by urethane bridges with thriethoxysilane groups,

– ESOR precursor obtained from tetramethoxysilane (TMOS) and 3-glycid oxypropyl trimethoxysilane (GLYMO),

– zirconium oxide precursor obtained by the sol-gel method.

Zirconium oxide matrix was used as an inorganic heteronetwork and as an efficient catalyst for the epoxy polymerization [38]. It should be noted that in the zirconium matrix prepared at 20–70 °C the number of unreacted epoxy groups is left (27–24%), which can be strongly diminished in the organic-inorganic matrix thanks to the reaction between epoxy groups and secondary amino groups in urethane linkage of DURS. Due to strong chemical bonding between organic and inorganic parts, the hybrid materials offer superior mechanical properties (elasticity, flexibility) and higher chemical stability. PbS nanoparticles were synthesized by reacting lead acetate with ammonium thiocyanate *in situ* with ZrO_2 or ZSUR matrices. The particle sizes responsible for the shift in absorption were controlled by the concentration of PbS (2–40 mol%) and by the temperature treatment ranging in 130–350 °C.

The structure and optical characterization of PbS NCs in ZrO_2 and ZSUR sol-gel films were investigated using TEM, absorption and photoluminescence spectra, the electrical measurements of current-voltage (*I-V*) characteristics and nitrogen adsorption technique.

2. Experimental

The following materials were used for the preparation of the final matrix of ZSUR:

– tetramethoxysilane (TMOS) $Si(OCH_3)_4$;

– 3-glycidoxypropyl trimethoxysilane (GLYMO)
$(CH_3O)_3 \equiv Si-(OC_3H_6)-CH_2-CH-CH_2$
O

– 3-isocyanatopropyl triethoxysilane (ICTEOS) $(C_2H_5O)_3Si-(C_3H_6)-N=C=O$,

– poly(ethylene glycol) (PEG) $HO-(CH_2-CH_2-O-)_n-H$

– zirconium (IV) n-propoxide, $Zr(OC_3H_7)_4$.

The final solution of ZSUR was obtained from ZrO_2 (N1 in Fig. 1) matrix, ESOR (N2 in Fig. 2) and DURS (N3 in Fig. 4) solutions. Each was prepared as shown in Figs. 1–3. The chart for the preparation of the final solution ZSUR (N4 in Fig. 4) doped
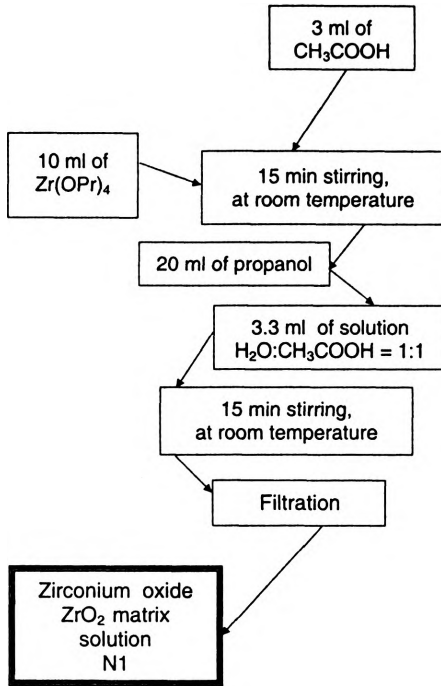
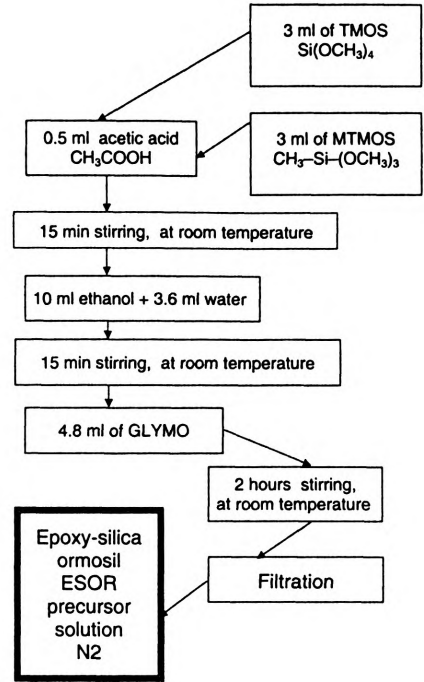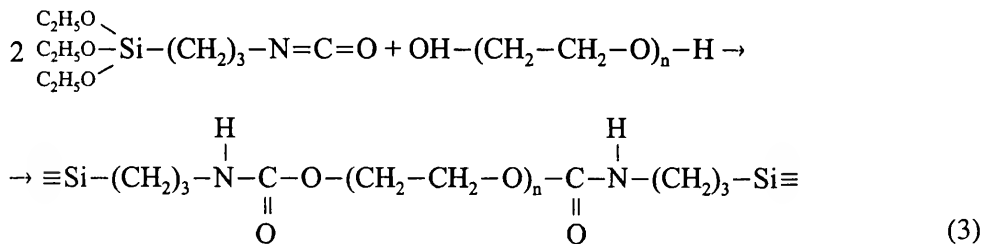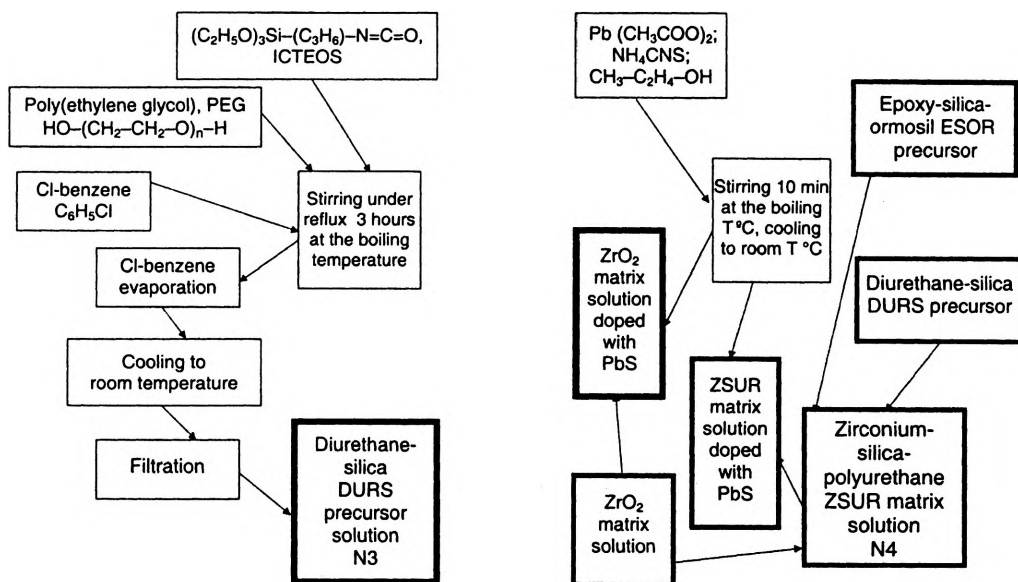Fig. 1. Chart for the preparation of the ZrO$_2$ matrix solution.

Fig. 2. Chart for the preparation of the ESOR matrix solution.

with PbS is presented in Fig. 4. PbS NCs doped thin films were prepared by dipping cleaned microscopic glass slides into final solutions of PbS-ZrO$_2$ or PbS-ZSUR. The DURS-olygomer solution was synthesized separately by reacting isocyanatopropyl triethoxysilane (ICTEOS) and poly(ethylene glycol) (PEG-600) with the molar ratio 2:1. The expected reaction of the synthesis of DURS can be discribed as follows:

$$2 \underset{C_2H_5O}{\overset{C_2H_5O}{C_2H_5O-Si}}-(CH_2)_3-N=C=O + OH-(CH_2-CH_2-O)_n-H \rightarrow$$

$$\rightarrow \equiv Si-(CH_2)_3-\overset{H}{\underset{|}{N}}-\overset{}{\underset{\parallel}{C}}-O-(CH_2-CH_2-O)_n-\overset{}{\underset{\parallel}{C}}-\overset{H}{\underset{|}{N}}-(CH_2)_3-Si\equiv$$
$$\qquad\qquad\qquad\qquad O \qquad\qquad\qquad\qquad\qquad O \qquad\qquad\qquad (3)$$

The reagents were stirred in chlorobenzene at boiling temperature under reflux for 3 hours. The residual solvent was evaporated and the DURS hybrid material olygomer was obtained. Isocyanate functionalized silane coupled with the polyol to form urethane linkage is known as a system improving bond strength.

The ESOR solution was obtained from TMOS and GLYMO with the molar ratio 1:1. First TMOS was hydrolyzed at room temperature (T_r) for two hours

▲
Fig. 3. Chart for the preparation of the DURS matrix solution.

Fig. 4. Flow chart for the preparation of the ZrO_2 and ZSUR matrices doped with PbS nanoparticles.

($TMOS:CH_3OH:H_2O:CH_3COOH = 15.0:12.8:7.2:2.4$), then GLYMO was added and stirred for 3 hours at T_r. Zirconium n-tetrapropoxide was hydrolyzed using a procedure similar to that reported in reference [35] and was added to DURS and ESOR solutions. Zirconium oxide is known as an effective catalyst for epoxy polymerization, the urethane's secondary amino group can also attack and convert the epoxy group into a protonated epoxide which is susceptible to any number of nucleophilic reagents. The nominal molar ratio in the final sol was $SiO_2:ZrO_2 = 69:31$, and of urethane to epoxy was 24:76.

The colloidal doping solution for PbS quantum dots was obtained separately from lead acetate and ammonium thiocyanate as it is shown in Fig. 4. The doping solution was added to the matrix solutions and the films were prepared by the dip-coating method. The reaction between lead and sulfur starts at about 140–170 °C thus PbS NCs are obtained *in situ* in the matrices. Various concentrations of PbS (2–40%) were obtained in ZrO_2 and ZSUR matrices. The films were dried at 40 °C and heated at 130–200 °C in case of ZSUR and at 200–350 °C in case of ZrO_2.

The color of the PbS NCs in ZrO_2 matrices (doped layers) varied from deep yellow to black-brown. The darkness of this color increased with an increase in the PbS NCs concentration and annealing temperature (T_{an}). On the contrary, the undoped ZrO_2 film remained colorless up to 350 °C.

Transmission electron microscopy measurements were performed with PHILIPS TECNAI 12 electron microscope, working at 100 kV and with a point resolution of 0.204 nm. Scratched fragments of the films doped with 20 mol% and 40% PbS were
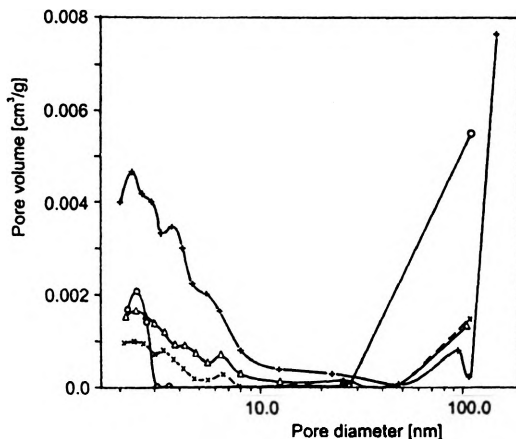
Fig. 5. Adsorption dV/dlog(D) pore volume. Pore diameter distribution obtained by BJH method for samples: ZSUR 40 °C (△△△) and 200 °C (∘∘∘); 2% PbS ZSUR 40 °C (+++) and 200 °C (×××).

deposited on a 300-mesh copper grid. The average diameter of PbS NCs was measured from TEM images evaluating about 100 particles.

The absorption spectra in the UV-VIS-NIR region were recorded at room temperature using Shimadzu UV-VIS spectrometer.

Photoluminescence measurement was carried out by exciting the samples with Ar$^+$ laser, while the output emission was detected by a cooled Si or Ge detector.

The experimental procedure of luminescent and electrical measurements were described earlier [35].

The porosity was estimated using the nitrogen adsorption technique. The specific surface area and pore size for multilayer adsorption was obtained from the BET method [39]–[41] which also provides a technique for estimating the pore volume for molecules of various sizes. Specific surface area and porosity were determined with the aid of a computer-controlled multifunctional ASAP 2010 apparatus (adsorption analyzer). Nitrogen adsorption experiments were performed at 77 K using a static volumetric method. The samples were previously degassed at 378 K for 6 hours. Nitrogen adsorption data were obtained using 0.15–0.2 g samples and successive doses of nitrogen. The algorithms used for interpretation of the measurements are ASAP 2010 apparatus implementation of the presented above methods. The total pore volume was estimated from nitrogen uptake at pressure P equal $0.99P_0$ (single point total pore volume). The pore size distribution has been calculated by the method of BJH [40] and is presented Fig. 5. The results of the temperature treatment of both the reference samples and the doped samples is a decrease in the pores volume and their specific area.

3. Results

Optical properties are directly related to the sizes of nanoparticles and can be extracted from the absorption spectra. Pure zirconium oxide and ZSUR films doped

with various concentrations of PbS nanoparticles were analyzed. Absorption spectra show the quantum confinement effect for both matrices (Figs. 6 and 7) and for all the doping concentrations. The stronger shift to shorter wavelength is obtained in films containing 5–20% of PbS indicating a smaller size of nanoparticles The direct band-gap energy of the PbS NCs was evaluated by fitting curves from Fig. 6a and Fig. 7a to the relation [24]

$$(\varepsilon\hbar\omega)^2 = \hbar\omega - E_g$$

where ε – absorption coefficient, E_g – optical band gap, $\hbar\omega$ – photon energy.

Band gaps (1.42–1.92 eV) of zirconium oxide films doped with 10–30 mol% of PbS NCs presented in Fig. 6b, and band gaps of PbS NCs in the ZSUR films ranging between 1.32–2.0 eV (for the concentrations 20–40% of PbS) as found in Fig. 7b, show a blue shift with respect to the bulk PbS (0.4 eV) material, due to size quantization.
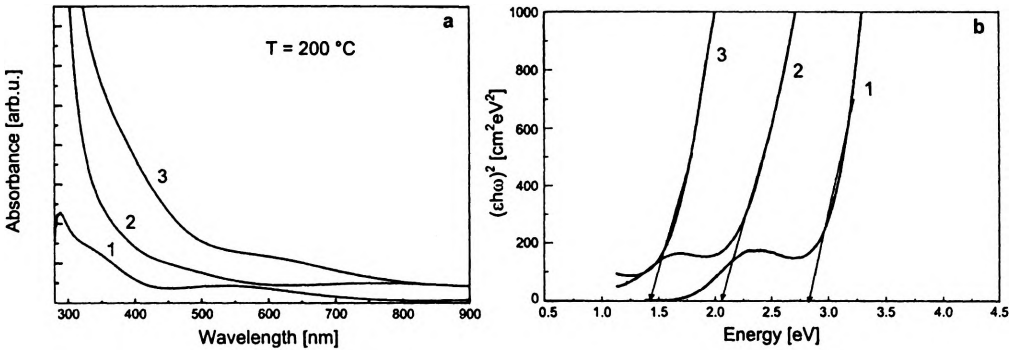

Fig. 6. Optical band edge of zirconium oxide films determined by absorption measurement: **a** – absorption spectra of ZrO_2 films doped with 1–10% (curve 1), 2–20% (curve 2) and 3–30% (curve 3) of PbS and annealed at 200 °C; **b** – $(\varepsilon\hbar\omega)^2$ *vs.* energy plots of absorption curves 1–3 in Fig. **a**.
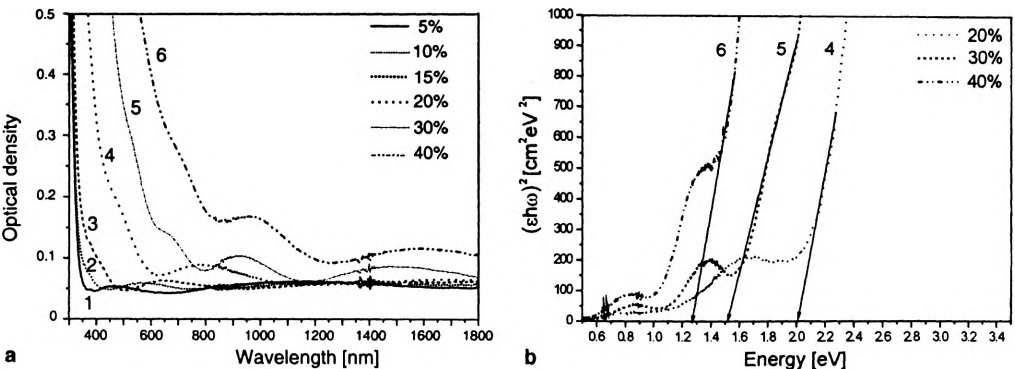

Fig. 7. Absorption spectra of ZSUR films: **a** – doped with different concentrations of PbS and annealed at 200 °C (curves 1–6); **b** – optical band edge of ZSUR films, determined by absorption measurement $(\varepsilon\hbar\omega)^2$ *vs.* energy plots of absorption (curves 4–6).
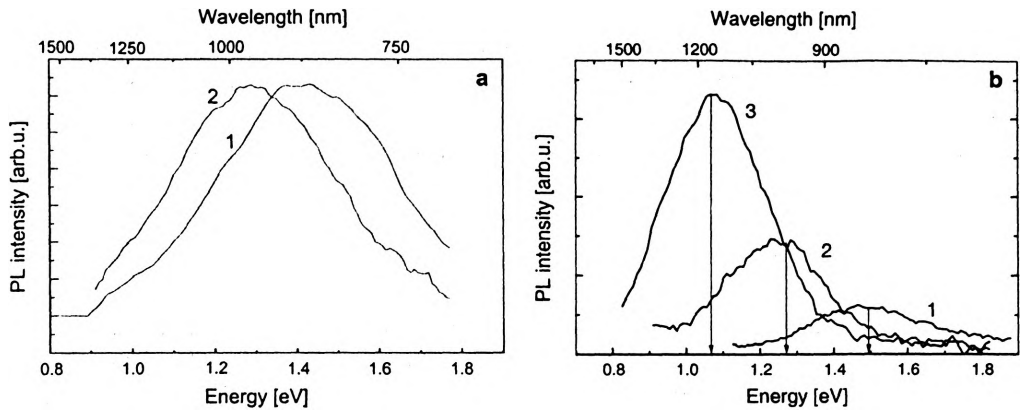
Fig. 8. PL spectra of ZSUR films: **a** – doped with 1–10% (curve 1) and 2–15% (curve 2) of PbS NCs treated at 200 °C, and **b** – ZrO$_2$ doped with 20% mole PbS NCs in the film, created at different T_{an}: 200 °C (curve 1), 250 °C (curve 2), 300 °C (curve 3).

The PL spectra of the investigated PbS NCs in ZrO$_2$ and ZSUR films are presented in Fig. 8. The quantum size effect can be observed clearly from the shift of luminescent peaks to higher energy with lowering concentration (from 15% to 10%) of PbS in ZSUR matrix (Fig. 8a) and with increasing annealing temperatures (from 200 °C to 300 °C) in ZrO$_2$ (Fig. 8b).

Table 1 summarizes the energy of the absorption edge as a function of annealing temperatures and mole percentage of PbS within the ZSUR and ZrO$_2$ matrices. It can be seen from this table that an increase in annealing temperature from 130 °C to 200 °C in ZSUR films and from 200 °C to 300 °C in ZrO$_2$ leads to an energy red shift of absorption edge. However, the annealing process above 200 °C (**a, b** in Tab. 1) and 300 °C (**c, d** in Tab. 1) does not cause further increase in the absorption edge and leads to the decomposition of PbS NCs. The band gap of the film (obtained at the

T a b l e 1. Optical properties of PbS nanoparticles in ZSUR and ZrO$_2$ sol-gel films.

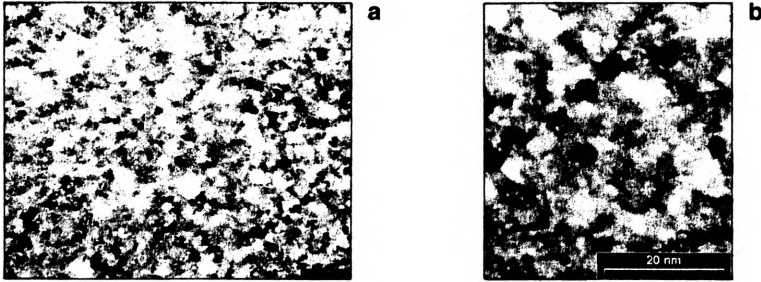| PbS [mol%] in ZSUR films	T_{an} [°C]	Absorption band edge [eV]	PbS [mol%] in ZrO$_2$ films	T_{an} [°C]	Absorption band edge [eV]
a. 20	130	2.75	d. 20	200	2.05
	170	2.30		250	1.65
	200	2.00		300	1.35
	220	2.25		350	1.92
b. 30	130	2.60	e. 30	200	1.55
	170	2.05		250	1.35
	200	1.52		300	1.65
	220	1.88		350	1.90
c. 40	130	2.15			
	170	1.72			
	200	1.28			
	220	1.85			

Fig. 9. TEM micrograph of ZrO_2 thin film doped with: **a** – 20% of PbS nanoparticles, **b** – with PbS NCs in which the crystallographic plane can be seen.
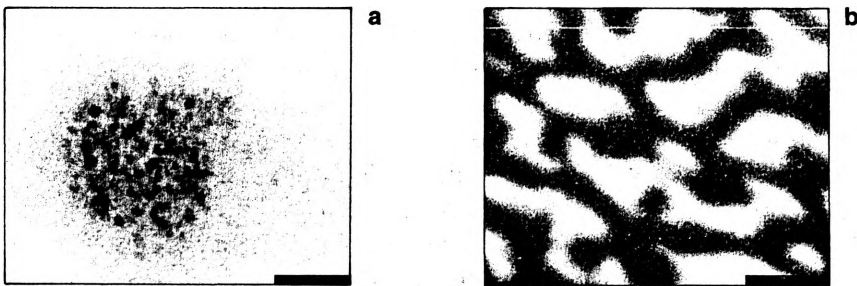

Fig. 10. TEM micrograph of ZSUR thin film: **a** – doped with 20% of PbS nanoparticles, **b** – TEM micrograph of ZSUR thin film doped with 40% of PbS nanoparticles.

T_{an} = 200 °C) with 20% PbS in ZSUR is very close to 20% of PbS in ZrO_2 (2.0 and 2.05 eV).

Microstructural characterization of investigated nanoparticles has been performed using TEM micrographs (Figs. 9 and 10). The average diameter of PbS NCs in the film heated to 200 °C and doped with 20 mol% of PbS in ZrO_2, as shown in Fig. 9, is 2–4 nm. One can see in Fig. 9 that PbS NCs have a nearly spherical shape and are homogeneously dispersed in an amorphous ZrO_2 thin film matrix. It should be noted here that, since the distances between the neighbouring NCs are few nanometers, carriers could be transferred from one NCs to another, either by hoping or tunneling.

The TEM micrographs (Fig. 10a, b) show that particle size in ZSUR matrix (4–8 nm for 20 mol% of PbS) are twice larger than in ZrO_2 matrix (2–4 nm). In the case of ZSUR matrix shown in Fig. 10b (40 mol% of PbS) we observed the growth of two kinds of PbS NCs, which can be associated with two growth processes. It can be seen that inorganic-organic copolymer exhibits phase separation of inorganic (ZrO_2) and organic parts. These processes can be responsible for the structure of ZSUR matrix, including ZrO_2 matrix in which smaller NCs are formed, and DURS organic matrix which is responsible for the interconnected network of the dark PbS.

Table 2 compares the band gap energies E_g between the uppermost valence band and the conduction band, and the shift in nanoparticles of well-known NCs materials.

T a b l e 2. Band gap energies E_g between the uppermost valence band and the conduction band, and the shift in nanoparticles.

Semiconductor	Structure	Band gap energies E_g [eV]	Shift (of E_g [eV]) in nanoparticles
CdS	Wurtzite	2.58	3.0 (after [22])
	Zinc blende	2.45	
CdSe	Wurtzite	1.84	2.2 (after [16])
	Zinc blende	1.67	
CdTe	Zinc blende	1.45	2.3 (after [19])
	Wurtzite	1.58	
PbS	Cubic	0.41	1.38–1.92 (after [35–37])

The band gap of PbS bulk 0.4 eV is shifted to 1.28–2.3 eV as obtained from absorption spectra due to the quantum size effect. A similar shift of the maximum is also observed in luminescent spectra.

The electrical properties of PbS NCs in the zirconia thin film were determined by the integration of this film in Au/PbS NCs-zirconia film/ITO structure, with NCs mol% of 15–30%. Figure 11a shows the experimental I-V characteristics of the investigated Au/PbS NCs-ZrO$_2$ thin films/ITO structures with different NCs density, while Fig. 11b demonstrates the I-V characteristics at various temperatures (70, 300 and 450 K). The inset of Fig. 11b shows the schematic diagram of the device structure, when the polarity of the voltage bias is defined as a positive front ITO with respect to the back Au contact (this configuration is used usually in optoelectronics devices) [35]. The average electric field intensity E in PbS NCs-ZrO$_2$ films, with thickness 50–300 nm, reaches 10^5–10^6 V/cm for a bias of several tens of volts. The PbS NCs-ZrO$_2$ thin films at low applied voltage exhibit high resistance of 10^7–10^{10} Ωcm, depending on the PbS NCs size (or annealing temperature), the PbS NCs density and the film thickness. It should be noted that the resistivity of the pure ZrO$_2$ film is about 10^{13} Ωcm. Figure 11a shows
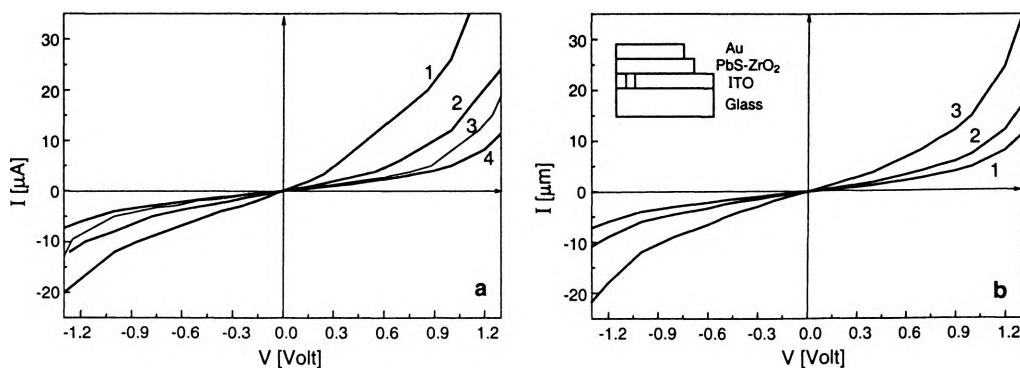

Fig. 11. Experimental I-V characteristic of PbS NCs in ZrO$_2$ film, measured at: **a** – room temperature of samples T_{an} = 250 °C and NCs mol% of 30% (curve 1), 25% (curve 2), 20% (curve 3), 15% (curve 4), and **b** – various temperatures: 70 K (curve 1), 300 K (curve 2), 450 K (curve 3).

that at electric fields between 0–0.7 V a linear *I-V* dependence is dominating, while at higher electric fields shows a nonlinear behavior [35]. The *I-V* characteristic also shows a non-symmetric behavior at high electric fields, pronounced as a larger current flow under the positive voltage *vs.* the negative branch (see Fig. 11**a**). The latter can be due to the differences in the work function of the electrode materials (Au at 4.3 eV and ITO at 4.7 eV).

The porosity was estimated using the nitrogen adsorption technique. The specific surface area and pore size for multilayer adsorption was obtained from the BET method which also provides a technique for estimating the pore volume for molecules of various sizes. The textural characteristics of the resultant gels were studied by means of N_2 physic absorption isoterms.

T a b l e 3. Porosity measurement of the ZSUR ormosil glasses doped with 2% PbS using the nitrogen adsorption technique.

	2% PbS/ZSUR, 40 °C	2% PbS/ZSUR, 200 °C	Reference ZSUR, 40 °C	Reference ZSUR, 200 °C
S_{BET} [m^2/g]	3.2	1.5	1.0	1.1
Total pore volume [cm^3/g]	0.0012	0.0005	0.0002	0.0001
Pore size by BET [nm]	1.54	1.41	0.78	0.37

Table 3 contains the results of nitrogen adsorption measurements – for the undoped ZSUR matrix (reference) and ZSUR doped with 2 mol% of PbS, and for the samples obtained at room temperature and treated to 200 °C. As we can see the reference samples show, both under treatment of 40 °C and 200 °C, low specific surface area of 1.0 m^2/g consistent with the low total pore volume. In the case of the doped samples the specific surface area increases by the factor of three at room temperature and then decreases. The results can be interpreted in the following way. The PbS nanocrystallites are creating an expansion of the part matrix surrouding the nanocrystallite. The surrounding tension is released again at high temperature resulting in the decrease of the pore volume and specific surface area.

4. Conclusions

Results of our experimental investigations may be summarized as follows:

1. The synthetic method which consists in the separate preparation of ZSUR matrix solution and PbS doping solution gives a possibility of the growth of PbS NCs with size ranging in 8–10 nm. Phase separation can be seen in TEM picture showing PbS nanoparticles and interconnected network of larger PbS clusters which are formed in ZSUR matrix structure including inorganic and organic parts.

2. The sizes of the particles were controlled by temperature treatment and by concentration of PbS. The quantum size effect is observed from both absorption and

emission spectra. The latter increased with an increase in the annealing temperature between 130–200 °C for ZSUR films and between 200–300 °C for zirconium oxide films.

3. The pore size of zirconium-ormosil doped with 2% of PbS as determined by BET is 1.54 nm. Dielectric measurements of the glasses are now in progress.

4. The device based on PbS-ZSUR composites may be of potential importance for ultrafast signal switching in integrated photonics.

References

[1] WOLFBEIS O., REISFELD R., OEHME I., Struct. Bonding **85** (1996), 51.

[2] BRINKER C.J., SCHERER G.W., *Sol-Gel Science*, Academic Press, New York 1990.

[3] BUCKLEY A.M., GREENBLATT M., J. Chem. Educ. **71** (1994), 599.

[4] PAJONK G.M., RAO A.V., PARVATHY N.N., ELALOUI E., J. Mater. Sci. **31** (1996), 5683.

[5] POPE E.J.A., MACKENZIE J.D., J. Non-Cryst. Solids **87** (1986), 185.

[6] SOREK Y., ZEVIN M., REISFELD R., HURVITS T., RUSCHIN S., Chem. Mater. **9** (1997), 670.

[7] ZEVIN M., REISFELD R., Opt. Mater. **8** (1997), 37.

[8] SARAIDAROV T., REISFELD R., PIETRASZKIEWICZ M., Chem. Phys. Lett. **330** (2000), 515.

[9] DE HAZAN Y., SHTER G.E., COHEN Y., ROTTMAN C., AVNIR D., GRADNER G.S., J. Sol-Gel Sci. Technol. **14** (1999), 233.

[10] DEL-MONTE F., CHEBEN P., GROVER C.P., MAKENZIE J.D., J. Sol-Gel Sci. Technol. **15** (1999), 73.

[11] REISFELD R., Struct. Bonding **85** (1996), 99. REISFELD R. [In] *Nonlinear Spectroscopy of Solids, Advances and Applications*, [Ed.] B. Di Bartolo, NATO ASI Series, Vol. 339, Series B, Physics, 1994, 491.

[12] GREGORKIEWICZ T., LANGER H.J.M., MRS Bulletin **24** (1999), 27.

[13] EKIMOV A.I., EFROS AL. L., ONUSHCHENKO A.A., Solid State Commun. **56** (1985), 921.

[14] ALIVISATOS A.P., Science **271** (1996), 933, and references therein.

[15] BEECROFT L.L., OBER C.K., Chem. Materials **9** (1997), 1302.

[16] LIFSHITZ E., DAG I., LITVIN I., HODES G., GORER S., REISFELD R., ZELNER M., MINTI H., Chem. Phys. Lett. **288** (1998), 188.

[17] MICIC O.I., SPARGUE J., LU S., NOZIK A.J., Appl. Phys. Lett. **68** (1996), 3150.

[18] MURRAY C. B., KAGAN C.R., BAWENDI M.G., Science **270** (1995), 1335.

[19] ZELNER M., MINTI H., REISFELD R., COHEN H., FELDMAN Y., COHEN S.P., TENNE R., J. Sol-Gel Sci. Technol. **20** (2001),153.

[20] REISFELD R., Proc. SPIE **1758** (1992), 546.

[21] GORER S., HODES G., SOREK Y., REISFELD R., Mater. Lett. **31** (1997), 209.

[22] ZELNER M., MINTI H., REISFELD R., COHEN H., TENNE R., Chem. Mater. **9** (1997), 2541.

[23] SPANHEL L., AGRAS E., SCHMIDT H., J. Non-Cryst. Solids **147–148** (1992), 657.

[24] WANG Y., SUNA A., MAHLER W., KASOWSKI R., J. Chem. Phys. **87** (1987), 7315.

[25] TRAKHTENBERG L.I., AXELROD E., GERASIMOV G.N., GRIGORIEV A.E., GRIGORIEV E.I., ZAVYALOV S.A., FELDMAN YU., Scientific Israel –Technological Advantages 1999, 1, 34.

[26] LIFSHITZ E., SIROTA M., PORTEANU H., J. Cryst. Growth **196** (1999), 126.

[27] MUKHERJEE M., DATTA A., CHAKRAVORTY D., Appl. Phys. Lett. **64** (1994), 1159.

[28] BORRELLI N.F., SMITH D.W., J. Non-Cryst. Solids **180** (1994), 25.

[29] MALYAREVICH A.M., SAVITSKI V.G., PROKOSHIN P.V., POSNOV N.N., YUMASHEV K.V., J. Opt. Soc. Am. B **19** (2002), 28.

[30] MARTUCCI A., INNOCENZI P., FICK J., MACKENZIE J.D., J. Non-Cryst. Solids **244** (1999), 55.

[31] NOGAMI M., NAGASAKA K., KOTANI K., J. Non-Cryst. Solids **126** (1990), 87.

[32] KUPRIANIDOU-LEODIDOU T., CASER W., SUTER U.W., J. Phys. Chem. **98** (1994), 8992.

[33] WEIMIN HUANG, JIANLIN SHAI, J. Mater. Res. **15** (2000), 11.

[34] MARTUCCI A., FIC J., SCHELL J., BATTAGLINI G., GUGLIELMI M., J. Appl. Phys. **86** (1999), 79.

[35] SASHCHIUK A., LIFSHITZ E., REISFELD R., SARAIDAROV T., ZELNER M., WILLENZ A., J. Sol-Gel Sci. Technol. **24** (2002), 31.

[36] SASHCHIUK A., LIFSHITZ E., REISFELD R., SARAIDAROV T., Mat. Sci. Eng. C **19** (2002), 67.

[37] SARAIDAROV T., REISFELD R., SASHCHIUK A., LIFSHITZ E., J. Sol-Gel Sci. Technol. **26** (2003), 1.

[38] PHILIPP G., SCHMIDT H., J. Non-Cryst. Solids **81** (1986), 31.

[39] BRUNAUER S., EMMETT P.H., TELLER E., J. Am. Chem. Soc. **60** (1938), 309.

[40] GREG S.J., SING K.S.W., *Adsorption, Surface Area and Porosity*, Academic Press, New York,1982.

[41] YARIV E., REISFELD R., SARAIDAROV T., AXELROD E., RYSIAKIEWICZ-PASEK E., WODNICKA K., J. Non-Cryst. Solids **305** (2002), 354.